Nonlinear Control Design and Stability Analysis of Single Phase Half Bridge Interleaved Buck Shunt Active Power Filter

Salwa Echalih*, Abdelmajid Abouloifa, Ibtissam Lachkar, Zineb Hekss, Abdelali El Aroudi, Fouad Giri, Mohammed Al-Numay

***Abstract*—This paper deals with nonlinear control of a single-phase half-bridge interleaved buck shunt active power filter (HBIB-SAPF) with a nonlinear load. The control objective for the system is twofold: performing power factor correction by compensating for harmonics and reactive current consumed by the nonlinear load from one hand and tightly regulating the HBIB converter DC capacitor voltage. Both objectives are accomplished using a two-loop nonlinear controller. The inner loop acts on the switching devices so that the active filter current tracks its reference with the aim of ensuring a unity power factor. This loop is tackled using backstepping technique and Lyapunov approach. The outer loop is responsible for regulating the DC capacitor voltage to its desired value, using a PI controller with a pre-filter. The stability analysis of the closed-loop system is formally performed by using the averaging theory. The validity of the designed nonlinear controller is checked by simulations in Matlab/SimpowerSystem showing its robustness and accuracy under various conditions.**

***Index Terms*—Nonlinear control design, Interleaved buck converter, Shunt active power filter, Lyapunov stability analysis, Averaging theory.**

I. Introduction

THE demand from the electricity customers for good quality of power supply is increasingly strict due to the rise of power electronics-based loads. This demand is often difficult to meet. The point is that these loads, such as variable speed machines, power converters, uninterruptible power supplies (UPS), involve nonlinear dynamics causing distortion of the power supply current. As a result, high-order harmonics and reactive current appear in the electrical supply system, leading to various undesirable effects such as degradation of power factor, equipment overheating, excessive transmission power losses, interference with proximity communication networks, distortion of the voltage at the point of common coupling (PCC) [1], [2], [3], [4].

(Corresponding author: Salwa Echalih.)

Salwa Echalih, Abdelmajid Abouloifa, Ibtissam Lachkar, and Zineb Hekss are with ESE Laboratory, ENSEM of Casablanca, Hassan II University of Casablanca, Casablanca 20103, Morocco (e-mail: salwa.echalih-etu@etu.univh2c.ma; a.abouloifa@gmail.com; lachkaribtissam@gmail.com; hekss.zineb@gmail.com).

Abdelali El Aroudi is with the Department of Electronics, Electrical Engineering and Automatic Control, Universitat Rovira i Virgili, 43002 Tarragona, Spain (e-mail: abdelali.elaroudi@urv.cat).

Fouad Giri is with NORMANDIE UNIV, UNICAEN, ENSICAEN, LAC, 14000 Caen, France (e-mail: fouadgiri@yahoo.fr).

Mohammed Al-Numay with Electrical Engineering Department, King Saud University, Saudi Arabia (e-mail: alnumay@ksu.edu.sa).

Active power filters (APF), based on VSI circuit, have been suggested and used in power utilities for dealing with harmonic pollution and improving the quality of power supply [5]. Many configurations of APFs are available on the market for industrial use, and out of them, a shunt APF (SAPF) is commonly employed as an effective tool to comply with harmonic standards such as IEEE-519 [6]. The SAPF is connected in parallel to the nonlinear load, injecting a suitable current at the PCC to simultaneously compensate for the adverse impacts of harmonics and reactive power imbalance [7], [8]. Nevertheless, this topology suffers from a dangerous phenomenon called a shoot through, which takes place when two switches of one leg are turned ON at the same time. As a matter of fact, system reliability and compensation effectiveness are eventually affected [9]. In practice, a dead time solution is used to handle this problem, but it has many disadvantages like output waveform distortion and complex control methods [10], [11].

The technology of interleaved buck converter (IBC) was developed as one of the most efficient means to overcome the above mentioned drawbacks, and it has been the purpose of most studies to date [12], [13], [14], [15], [16]. The basic unit of this topology is a buck converter with a unidirectional power flow where the bridge consists of one controllable switch in series with one diode. Compared to the conventional VSI, IBC has the advantage of being free from the shoot-through concern, which can immediately avoid the requirement of a dead time. Moreover, the converter efficiency is drastically enhanced, the voltage and current stresses are decreased, and the life-time of the converter circuit is also extended.

Over the last years, interleaved buck converter has been presented as a filtering system and has attracted considerable attention due to its excellent compensation performance, high reliability, and low control complexity. The available interleaved buck SAPFs exist in two variants: half-bridge and full-bridge. The half-bridge interleaved buck SAPF (HBIB-SAPF) enjoys several practical advantages compared to a full bridge topology. Indeed, it involves fewer switches and coupling inductors, which results in reduced control functions, lower cost, and ease of control [17], [18].

The problem of controlling interleaved buck SAPF has been previously treated with different control methods, which can be roughly classified into four categories. The first uses hysteretic current regulator based on the harmonic extraction methods and fuzzy logic control. However, it is restricted to

three wire systems and four wire three phase SAPF [19], [20], [21], [22], [23], [24]. This method does not use the exact nonlinear model of the HBIB-SAPF in the control design, and thus the knowledge of the system's nonlinear behavior is missed. In addition, the techniques applied for generating the compensation current reference are very complex and entail onerous implementation. In [18], harmonic mitigation and reactive power compensation for single-phase HBIB-SAPF have been addressed, using a half-wave control strategy with PI regulator. The second category of approaches includes the use of hybrid control based on the hybrid automata theory [17], [25], [26]. The third category of methods is limited to the intelligent control techniques such as particle swarm optimization (PSO) and enhanced (PSO) algorithm, which have been proposed for the three phase SAPF system whose performances have been shown by experimental results [27], [28]. The last category includes the nonlinear regulator (e.g. [29]), where the authors suggested a multitudinal sliding mode control (MSMC) to stabilize the DC link voltage, and a hysteretic band modulation method to generate gate signals for the single-phase full-bridge interleaved buck converter. However, the main disadvantage of this modulation technique is the fact that the switching frequency is not fixed making the switching ripple current filtering a difficult task and introducing thus the switching noise to the power grid. Besides, this frequency can also make the power switch uncontrolled under some conditions. A common drawback in most of the previous works is that no formal analysis was performed for proving the closed-loop system stability and to show that the proposed regulators actually achieve the objectives they were designed for.

This paper addresses the nonlinear control of a single-phase half-bridge interleaved buck SAPF in presence of nonlinear loads. In most industrial applications, three-phase loads are used [30]. But in practical situations, it turns out that implementing a single SAPF at each phase is more efficient, than using a higher-power three-phase SAPF [4], [31], [29], [17]. This study seeks a control strategy that will ensure the achievement of two main objectives simultaneously: i) Compensation for reactive energy and harmonics caused by the nonlinear load; ii) Regulation of the capacitor voltage at the HBIB converter. For that, the design of the nonlinear controller is performed based on the mathematical averaged model of the whole system, which guarantees a smoother control and better actuator protection, in contrast to previous controllers presented in [17], [18], [32], [29]. The suggested controller consists of a cascaded double-loop. In the inner loop, the current controller is performed using backstepping and Lyapunov techniques in order to deal with harmonics compensation. The outer loop regulator is built-up based on a PI controller with a pre-filter to maintain the DC bus voltage of the HBIB converter to a desired level. It is worth noting that this proposed control strategy is developed following the indirect current control viewpoint, in which no harmonic detection algorithm was used to generate the filter current references, comparing with most existing approaches such in [19], [20], [21], [22], [23], [24], [28]. This study is also supported by two analyses: The first analysis is concerned with the behavior of the system in steady state. The second is a rigorous analysis that relies on the averaging theory as a tool for evaluating the closed-loop system's stability and showing the theoretical realization of all desired objectives, unlike the former research in which no such analysis has been formally performed. Moreover, numerous simulations are carried out under different working conditions. The performance effectiveness and robustness of the proposed nonlinear controller are compared with a hybrid controller under load changes.

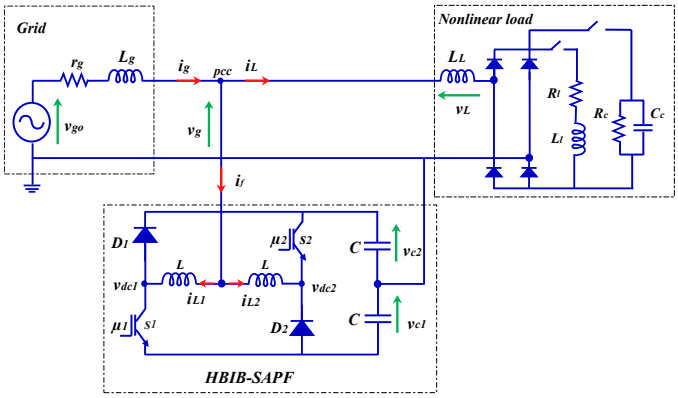

Fig. 1. Schematic circuit diagram of a single-phase HBIB-SAPF.

The remainder of the paper is organized as follows: The description and mathematical modeling of the system considered in this study are presented in Section 2. The steady state analysis is provided in Section 3. The design of the nonlinear controller is developed in Section 4, the closed-loop control system is formally analyzed in Section 5. Section 6 presents and discusses the outcomes of numerical simulations performed on the HBIB-SAPF system with the designed nonlinear controller. Finally, the conclusion is given in Section 7.

II. System description and mathematical modeling

The proposed system configuration of a single-phase HBIB-SAPF is shown in figure 1. The converter topology is, in principle, composed of two individual buck circuits, forming two legs determined with two split capacitors of energy storage (C_1, C_2). Each bridge consists of one switch and one diode that are connected in series, plus one inductor. These interfacing inductors (L_1, L_2) serve to implement the HBIB-SAPF with a nonlinear load in parallel to the power grid which is represented by a series connection of a sinusoidal voltage source and an internal impedance (r_g, l_g).

The interleaved buck converter works in accordance with the half cycle PWM on the basis of the filter current [18]. Hence, during the positive half cycle, the first limb (s_1, D_1, L_1) operates whereas the second limb (s_2, D_2, L_2) operates at the negative half cycle.

A. System model

To simplify the model of HBIB-SAPF, the following assumption is considered.

Assumption 1. *Assuming that the two buck circuits are identical. This involves the following equalities:*

- $L_1 = L_2 = L$;
- $C_1 = C_2 = C$.

Firstly, let γ the signal defined as follows

$$\gamma = \text{sgn}(i_f) = \begin{cases} +1 & \text{if} \quad i_f(t) > 0 \\ -1 & \text{if} \quad i_f(t) < 0 \end{cases} \tag{1}$$

where sgn stands for the signum function.

With the use of Kirchhoff's laws applied to the HBIB-SAPF, the loop equation is represented as follows

$$v_g = (L\frac{di_{L1}}{dt} + v_{dc1})\frac{1+\gamma}{2} + (L\frac{di_{L2}}{dt} + v_{dc2})\frac{1-\gamma}{2} \tag{2}$$

Define μ_i $(i = 1, 2)$ as binary control input signals for interleaved buck converter that take values in the finite set $\{-1, 1\}$ according to the following expression:

$$\mu_i = \begin{cases} +1 & S_2 \text{ ON, } S_1 \text{ OFF} \\ -1 & S_2 \text{ OFF, } S_1 \text{ON} \end{cases}$$

The middle point voltage of the two legs can be expressed as follows:

$$\begin{aligned} v_{dc1} &= v_{c1}\frac{\mu_1 - 1}{2} + v_{c2}\frac{\mu_1 + 1}{2} \\ v_{dc2} &= v_{c1}\frac{\mu_2 - 1}{2} + v_{c2}\frac{\mu_2 + 1}{2} \end{aligned} \tag{3}$$

By substituting (3) into (2), we obtain the following equation:

$$\begin{aligned} v_g = L\frac{di_{L1}}{dt}\frac{1+\gamma}{2} + v_{c1}\frac{\mu_1 - 1}{2}\frac{1+\gamma}{2} + v_{c2}\frac{\mu_1 + 1}{2}\frac{1+\gamma}{2} + \\ L\frac{di_{L2}}{dt}\frac{1-\gamma}{2} + v_{c1}\frac{\mu_2 - 1}{2}\frac{1-\gamma}{2} + v_{c2}\frac{\mu_2 + 1}{2}\frac{1-\gamma}{2} \end{aligned} \tag{4}$$

when

$$\begin{cases} \gamma = +1 \quad \frac{di_{L1}}{dt} \neq 0 \quad \text{and} \quad \frac{di_{L2}}{dt} = 0 \\ \gamma = -1 \quad \frac{di_{L1}}{dt} = 0 \quad \text{and} \quad \frac{di_{L2}}{dt} \neq 0 \end{cases}$$

Therefore, the first and fourth terms of (4) are equivalent to:

$$L\frac{di_{Li}}{dt}\frac{1 \pm \gamma}{2} = L\frac{di_{Li}}{dt} \qquad i = 1, 2 \tag{5}$$

The filter current can be written, according to the inductor currents $i_{L1}(t)$ and $i_{L2}(t)$, as follows:

$$i_f = i_{L1} + i_{L2} \tag{6}$$

From the above equations, the switched model of HBIB-SAPF is then as follows:

$$L_g\frac{di_g}{dt} = -r_g i_g + v_{go} - v_g \tag{7a}$$

$$L\frac{di_f}{dt} = -v_{c1}\frac{\mu - 1}{2} - v_{c2}\frac{\mu + 1}{2} + v_g \tag{7b}$$

$$C\frac{dv_{c1}}{dt} = i_f\frac{\mu - 1}{2} \tag{7c}$$

$$C\frac{dv_{c2}}{dt} = i_f\frac{\mu + 1}{2} \tag{7d}$$

with

$$\mu = \mu_i = \begin{cases} +1 & S_2\text{ON}, S_1\text{OFF} \\ -1 & S_2\text{OFF}, S_1\text{ON} \end{cases}$$

Since μ represents a discontinuous control input signal in the model given by (7a)-(7d), the design of a continuous control law cannot be performed. To overcome this handicap, the next step is to obtain the averaged model. To obtain such a model, moving averaging of the electrical variables and the control signals is carried out over each switching period. The obtained average model is as follows:

$$L_g\frac{dx_1}{dt} = -r_g x_1 + v_{go} - v_g \tag{8a}$$

$$L\frac{dx_2}{dt} = -x_3\frac{u - 1}{2} - x_4\frac{u + 1}{2} + v_g \tag{8b}$$

$$C\frac{dx_5}{dt} = x_2 u \tag{8c}$$

$$C\frac{dx_6}{dt} = -x_2 \tag{8d}$$

where $x_1, x_2, x_3, x_4, x_5, x_6$, and u stand for the time average values over one switching period of the variables i_g, i_f, v_{c1}, v_{c2}, $(v_{c1} + v_{c2})$, $(v_{c1} - v_{c2})$, and the control signal μ, respectively.

III. Steady state analysis

The grid voltage is considered sinusoidal signal. This can be expressed as follows:

$$v_{go} = E_g \sin(\omega_g t) \tag{9}$$

with E_g and ω_g are the magnitude and the angular frequency of the power grid respectively.

We aim that, in steady-state, the grid current i_g follows a sinusoidal template which is in phase with the voltage v_g. Therefore, x_1 is given by:

$$x_1 = \beta E_g \sin(\omega_g t) \tag{10}$$

Substituting (9)-(10) into (8a), one can easily obtain:

$$\bar{v}_g = V_g \sin(\omega_g t - \theta_1) \tag{11}$$

Where

$$V_g = E_g\sqrt{(L_g\beta\omega_g)^2 + (1 - r_g\beta)^2}$$

$$\theta_1 = \arctan\left(\frac{L_g\beta\omega_g}{1 - r_g\beta}\right)$$

The filter current that will be injected by the HBIB-SAPF into the grid, in the steady state operation, is given by:

$$x_2 = x_1 - i_L \tag{12}$$

where the, in steady-state, load current i_L is a periodic signal that can be expanded as a Fourier series

$$i_L = \sum_{h=1}^{\infty} I_{Lh} \sin(h\omega_g t + \varphi_h) \tag{13}$$

where I_{Lh} and φ_h stand for the magnitude and the phase of h^{th} harmonic element of the load current, respectively.

Based on (13) and using (10), x_2 can be expressed as follows:

$$x_2 = I_f \sin(\omega_g t - \theta_2) - \sum_{h=2}^{\infty} I_{Lh} \sin(h\omega_g t + \varphi_h) \tag{14}$$

with

$$I_f = \sqrt{(I_{L1}\sin(\varphi_1))^2 + (\beta E_g - I_{L1}\cos(\varphi_1))^2}$$

$$\theta_2 = \arctan\left(\frac{I_{L1}\sin(\varphi_1)}{\beta E_g - I_{L1}\cos(\varphi_1)}\right)$$

Based on (8b), we deduce that:

$$\bar{v}_f = v_g - L\dot{x}_2 \tag{15}$$

Using (11) and (14), one obtains:

$$\bar{v}_f = V_f \sin(\omega_g t - \theta_3) - L\omega_n \sum_{h=2}^{\infty} I_{Lh} h \sin(h\omega_g t + \varphi_h) \tag{16}$$

where

$$V_f = \sqrt{(\Phi_1)^2 + (\Phi_2)^2}$$

$$\Phi_1 = V_g \sin(\theta_1) + LI_f\omega_g \cos(\theta_2)$$

$$\Phi_2 = V_g \cos(\theta_1) - LI_f\omega_g \sin(\theta_2)$$

$$\theta_3 = \arctan\left(\frac{\Phi_1}{\Phi_2}\right)$$

Using (8c)-(8d), the following differential equation is obtained:

$$C\frac{d(x_3^2 + x_4^2)}{dt} = x_2\bar{v}_f \tag{17}$$

Define a new variable $\Psi = x_3^2 + x_4^2$ and substitute (14) in the above equation. This results in the following equation:

$$C\frac{d\Psi}{dt} = f(\beta) - g(\beta)\cos(2\omega_g t - \theta_2 - \theta_3) - L\omega_g \sum_{h=2}^{\infty} (I_{Lh}h)^2 \sin^2(h\omega_g t + \varphi_h) \tag{18}$$

where

$$f(\beta) = \frac{I_f V_f}{2}\cos(\theta_3 - \theta_2) \text{ and } g(\beta) = \frac{I_f V_f}{2}$$

Remark 1: The DC bus voltage contains a DC term and harmonics at multiple integer of the double grid frequency.
By averaging (18) during the grid period, the following averaged equation is obtained:

$$C\frac{d\bar{\Psi}}{dt} = f(\beta) \tag{19}$$

Remark 2: In steady state, ($\frac{d\bar{\Psi}}{dt} = 0$). Consequently, the power processed by the HBIB-SAPF is completely transferred to the load.
By solving (19) for $\bar{\Psi}$, one obtains:

$$\bar{\Psi} = \frac{1}{C} f(\beta)t + \bar{\Psi}(0) \tag{20}$$

where $\bar{\Psi}(0)$ indicates the square of the DC voltage at the initial time. According to (20), the time evolution of the DC bus voltage ($x_5 = x_3 + x_4$) in steady-state is fully maintained by the term $f(\beta)$. This may increase or decrease the DC bus voltage and thus may destabilize the entire system. Consequently, the control signal β should be generated by the outer loop which guarantees the equality $f(\beta) = 0$ and thereby preserving the overall stability of the system.

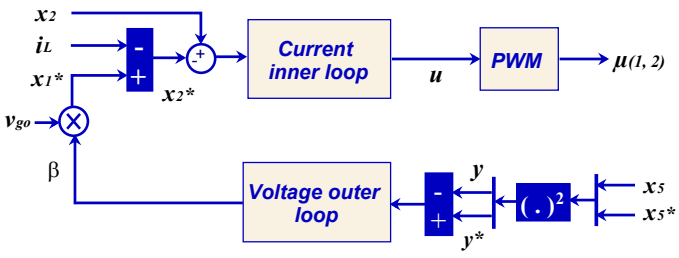

Fig. 2. Schematic diagram of the designed controller.

Based on $v_f = [(u-1)x_3 + (u+1)x_4]/2$ and using (19), the control law u^* that enables the requirement of power factor correction is given by:

$$u^* = 2\frac{V_f}{x_5}\sin(\omega_g t - \theta_3) \tag{21}$$

In practical use, V_f is very close to E_g (r_g, L_g and L are neglected) and since the control signal $u^* \in [-1, 1]$, we can conclude this condition:

$$x_5 > 2E_g \tag{22}$$

The obtained result shows that the HBIB-SAPF can operate properly when the DC bus voltage is strictly higher than twice the amplitude of the grid voltage.

IV. Two-loop controller design

This section is devoted to the nonlinear control design for single-phase half-bridge interleaved buck SAPF. The controller will ensure two main objectives; firstly, performing PFC and secondly, regulating the DC capacitor voltage to its desired reference v_{dc}^*. The PFC is achieved by compensating for harmonic and reactive current generated by the nonlinear load. In order to achieve the desired control aims, two nonlinear cascaded-loops were developed i.

i. The inner current loop for performing PFC.
ii. The outer voltage loop for regulating the voltage at the DC side of the HBIB-SAPF.

Figure 2 shows the block diagram of the proposed two-loop controller where the inner loop is developed using a backstepping approach with the Lyapunov stability argument, whereas the voltage outer loop is implemented utilizing a PI controller with a pre-filter.

A. Current reference extraction

Since the main goal of the active power filter is to compensate for harmonics and reactive power simultaneously, it must be current-controlled to accurately track the reactive and harmonic currents induced by the nonlinear load. To do this, an estimate of these components is needed. Several methods

have been employed, but they imply a complex calculus that requires powerful processing units in the hardware implementation. Here, the problem is applied in a different way. Indeed the objective is to shape the grid current so that to be a sine wave signal in phase with the sinusoidal grid voltage. To this end, the grid current should track its reference signal which can be expressed as follows:

$$x_1^* = \beta v_{go} \tag{23}$$

where β is a suitable positive time varying conductance. As the control is performed on the filter current x_2 related to the grid current x_1. It follows that the control law to be implemented must ensure a tracking between x_2 and its reference x_2^* defined by:

$$x_2 = x_1 - i_L \tag{24a}$$
$$x_2^* = x_1^* - i_L \tag{24b}$$

B. Current inner loop

To achieve the PFC requirement, one seeks to control the current x_2 generated by the HBIB-SAPF to track, to the best as possible, its reference x_2^* given by (24b). To accomplish this, the inner controller will now be designed using Backstepping approach and Lyapunov design.

Let us introduce the current tracking error z_1 for the interleaved buck SAPF that is defined by:

$$z_1 = L(x_2 - x_2^*) \tag{25}$$

Using (8b) and (24b), the dynamics of z_1 is given by

$$\dot{z}_1 = -\frac{1}{2}ux_5 + \frac{1}{2}x_6 + \bar{v}_g - L\dot{x}_1^* + L\frac{di_L}{dt} \tag{26}$$

Notice that the control signal u has appeared in (26) after time differentiation of the tracking error z_1. A suitable control law for the synthesis of the control signal u must be now determined such that the z_1 dynamics is globally asymptotically stable. Consider the Lyapunov function candidate and its derivative, respectively given by:

$$V_1 = \frac{1}{2}z_1^2 \tag{27a}$$
$$\dot{V}_1 = z_1\dot{z}_1 \tag{27b}$$

This shows that, for the z_1 dynamics defined by (26) to be globally asymptotically stable, it is enough to choose the control law u so that $\dot{V}_1 = -k_1 z_1^2$ which, owing to (27b), amounts to assure the following equality:

$$\dot{z}_1 = -k_1 z_1 \tag{28}$$

At this point, k_1 is a positive design parameter of the controller.

Combining (26) and (28) one obtains the following equation defining the backstepping control law:

$$u = \frac{2}{x_5}\left[\frac{1}{2}x_6 + \bar{v}_g - L\dot{x}_1^* + L\frac{di_L}{dt} + k_1 z_1\right] \tag{29}$$

The obtained control law (29) will be applied to the half cycle PWM [18] for generating a binary gate signals to the HBIB converter.

Proposition 1. *Consider the system depicted in figure 1, whose average model is given in* (8a)-(8d)*, together with the control law* (29)*. If β and its time derivative $\dot{\beta}$ are available, the z_1-coordinate of the inner loop is described by the following equation:*

$$\dot{z}_1 = -k_1 z_1 \tag{30}$$

Consequently, the error is globally asymptotically vanishing.

Remark 3: Thus far, it is necessary and sufficient that β and $\dot{\beta}$ be available in order to achieve the PFC aim. To this end, in the next subsection, β will be provided by the external responsible loop for regulating the DC voltage across the split capacitor of the HBIB converter.

C. Voltage outer loop

As detailed in the steady state analysis (Section III), regulating the DC bus voltage is necessary for maintaining the power balance of the overall system. To reach this purpose, the signal β is generated by an external loop that is responsible for regulating the output voltage x_5 to its desired reference x_5^*.

i. *Relation between β and x_5:*

A relation between the signal β and the output voltage x_5 is initially established in the proposition below.

proposition 2. *Consider the HBIB-SAPF of figure 1 whose model is given in* (8a)-(8d) *with the inner control law defined by* (29)*. One has the following statement*
The variable $y = x_5^2$ which is the squared DC voltage is related to the signal β according to the following first-order differential equation

$$\frac{dy}{dt} = 2\left[f_1(\beta, \dot{\beta}) + f_2(\beta, \dot{\beta}, z_1, t)\right] \tag{31}$$

where the expression of $f_1(\beta, \dot{\beta})$ and $f_2(\beta, \dot{\beta}, z_1, t)$ are detailed in Appendix.

proof. *By replacing the control law* (u) (29) *in* (8c)*. Then, one gets:*

$$\frac{dx_5}{dt} = \frac{1}{x_5}\left[f_1(\beta, \dot{\beta}) + f_2(\beta, \dot{\beta}, z_1, t)\right] \tag{32}$$

The expression (31) *is thus obtained by time differentiation of y and using (30).*

ii. *Squared DC voltage:*

The control law generated from the outer loop should be appropriately tuned such that the variable $y = x_5^2$ is regulated to its desired reference given by $y^* = x_5^{*2}$. However, it is necessary to bear in mind that β and $\dot{\beta}$ should be available (see Remark 2). In view of these facts, we consider the following first-order filtered PI controller expressed in the s domain:

$$\beta = \frac{k_2}{k_2 + s}(k_p Z_2(s) + k_i Z_3(s)) \tag{33}$$

TABLE I
NOTATIONS FOR RESULTS FORMULATION.

$$z_1 = L(x_2 - x_2^*); \qquad z_2(t) = y^*(t) - y(t); \qquad z_3(t) = \int_0^t z_2(\tau)d\tau; \qquad z_4 = \beta; \qquad \beta_0 = \frac{b_2 + \sqrt{b_2^2 - 4b_1b_3}}{2b_1}; \qquad \varepsilon = 1/\omega_g;$$

$$b_1 = r_g E_g; \qquad b_2 = E_g + (r_g\cos(\varphi_1) + (L_g + L)\omega_g \sin(\varphi_1))\, I_{L1}; \qquad b_3 = I_{L1}\cos(\varphi_1); \qquad b_4 = \frac{E_g}{C}(L_g + L)\left[\beta_0 E_g - I_{L1}\cos(\varphi_1)\right];$$

$$b_5 = \frac{E_g}{C}\Big[\,(1 - r_g\beta_0)\, E_g + (L_g + L)\omega_g I_{L1}\sin(\varphi_1) + ((L_g + L)k_2 - r_g)\,(\beta_0 E_g - I_{L1}\cos(\varphi_1))\,\Big]; \qquad a_0 = k_1k_ik_2(b_5 - k_2b_4);$$

$$a_1 = k_2\{k_i(b_5 - k_2b_4) + k_1[k_pb_5 - (k_pk_2 + k_i)b_4]\}; \qquad a_2 = k_2[k_p(b_5 - k_2b_4) - k_ib_4 + k_1(1 - k_pb_4)]; \qquad a_3 = k_1 + k_2(1 - k_pb_4).$$

with

$$z_2(t) = y^*(t) - y(t), \quad z_3(t) = \int_0^t z_2(\tau)d\tau$$

where $Z_2(s)$ and $Z_3(s)$ stand for the Laplace transforms of the variables $z_2(t)$ and $z_3(t)$ respectively. The regulator parameters (k_2, k_p, k_i) are suitable positive coefficients. In the forthcoming analysis, it will be shown how these design parameters should be chosen to ensure that the control objectives are achieved. At this point, notice that (33) entails that the dynamics of β can be described by the following equation:

$$\dot{\beta} = k_2(k_pz_2 + k_iz_3 - \beta) \tag{34}$$

V. CONTROL SYSTEM ANALYSIS

The stability analysis of the global closed-loop system is demonstrated in this section using some analysis tools such as the averaging theory [33], indirect Lyapunov stability, and Routh-Hurwitz criterion. The notations given in Table I are required for formulating the results.

The following theorem shows that all control objectives are reached in the average with an accuracy that depends on the grid frequency ω_g.

Theorem (main result). *Consider the half-bridge interleaved buck SAPF shown in figure 1, represented by the model* (8a)-(8d) *with the nonlinear cascade controller, consisting of*

- *The current inner compensator defined by the control law* (29) *with k_1 a positive parameter .*
- *The voltage outer regulator described by the control law* (33) *with (k_2, k_p, k_i) positive constants.*

Then, the system has the following properties in closed-loop operation

1) The current error $z_1 = L(x_2 - x_2^*)$ vanishes exponentially fast (where $x_2^* = \beta v_{go} - i_L$).
2) Introduce the following state vector:

$$Z = \begin{pmatrix} z_1 & z_2 & z_3 & z_4 \end{pmatrix}^T$$

The state vector Z is governed by the following differential equation:

$$\dot{Z} = \rho(t, Z) \tag{35}$$

where ρ is given by the following expression:

$$\rho(t, Z) = \begin{pmatrix} -k_1z_1 \\ -f_1(Z) - f_2(Z, t) \\ z_2 \\ k_2(k_pz_2 + k_iz_3 - z_4) \end{pmatrix}$$

3) Assume the controller design parameters (k_1, k_2, k_p, k_i) are selected so that to fulfill the following inequalities:

$$a_0 > 0,\ a_3 > 0,\ a_2a_3 - a_1 > 0,\ a_1a_2a_3 - a_1^2 - a_0a_3^2 > 0 \tag{36}$$

Then, there exist $\varepsilon^* > 0$ and $\eta^* > 0$ such that $\forall\varepsilon$ such that $0 < \varepsilon < \varepsilon^*$, the system (35) has a unique exponentially stable $\frac{\pi}{\omega_g}$-periodic solution $\bar{Z}(t, \varepsilon)$ satisfying $\|\bar{Z}(t, \varepsilon) - Z_0^*\| < \eta^*\varepsilon$ with $Z_0^* = \begin{pmatrix} 0 & 0 & \frac{\beta_0}{k_i} & \beta_0 \end{pmatrix}$

Remark 4:

1) *Equations* (33)-(34) *guarantee that β and its time derivative $\dot{\beta}$ may be computed by making use of the available signals. Then, according to Proposition 1, the current error z_1 is governed by* (30)*. This is a differential equation representing a globally asymptotically stable. Hence z_1 vanishes exponentially.*
2) *The state vector* (35) *is immediately attained from* (28)*,* (31)*,* (33) *and* (34)*.*
3) *The above theorem indicates that, under condition* (36)*, the compensation of reactive and harmonic currents (PFC requirement) is actually achieved in the average with an accuracy depending on the value of $\varepsilon = 1/\omega_g$. Furthermore, The theorem also ensure that $z_4 = \beta$ converges to a constant value β_0, assuring thus the achievement of the PFC aim after a transient period. Moreover, since $z_2 = y^* - y$, the tracking objective relating to the DC bus squared voltage is effectively ensured in the average with an accuracy according to the voltage grid frequency ω_g. The higher the grid frequency, the increased accuracy. Thus, the used frequency $\omega_g = 50\,\text{Hz}$ allows for tight voltage regulation and good PFC quality.*
4) *It is worth noting that the power stage circuit connected to the grid which is represented by* (7) *is 4^{th} order. However, the first equation in* (7) *corresponding to the grid dynamics is uncoupled from the dynamics of the HBIB-SAPF. Note also that* (7b) *describes the current i_f which is the sum of both i_{L1} and i_{L2}. Therefore, the*

model of the power stage to be controlled is 3^{th}order. Besides, consider that the inner current loop uses a static current control law (29) *and it adds no new state variable to the system. Meanwhile, the outer voltage controller formed by a filtered PI add two new state variables which makes the closed-loop system of 5^{th} order. Note that the averaged equations of* (8c) *and* (8d)*, we can observe that if x_2 converges to zero in average then x_6 will be automatically bounded (x_6 converges to a constant (up to ripples)). Therefore, x_6 was not taken into account and the model used to perform stability analysis is 4^{th} order.*

proof of Theorem. Below, a stability analysis will be performed for (35) after using the averaging theory [33]. For this purpose, first a time-scale change $\tau = \omega_g t$ is introduced. Then, it can readily be seen from (36) that $W(\tau) \overset{\text{def}}{=} Z(t) = Z(\tau/\omega_g)$ is governed by the differential equation:

$$\dot{W}(\tau) = \varepsilon\psi(\tau, W, \varepsilon) \tag{37}$$

where

$$\psi(\tau, W, \varepsilon) = \begin{pmatrix} -k_1 w_1 \\ -\psi_1(W) - \psi_2(W, \tau, \varepsilon) \\ w_2 \\ k_2(k_p w_2 + k_i w_3 - w_4) \end{pmatrix} \tag{38}$$

with

$$\psi_1(W(\tau)) \overset{\text{def}}{=} f_1(Z(t)) = f_1(W(\tau));$$
$$\psi_2(W(\tau), \tau, \varepsilon) \overset{\text{def}}{=} f_2(Z(t), t) = f_2(W(\tau), \varepsilon\tau).$$

It stands out from (31) and (38) that $\psi(\tau, W, \varepsilon)$ as a function of τ is periodic with period 2π. Let us now introduce the average function:

$$\psi_0(W_0) \overset{\text{def}}{=} \lim_{\varepsilon\to 0} \frac{1}{2\pi} \int_0^{2\pi} \psi(\tau, W_0, \varepsilon) d\tau,\ W_0 \in \mathbb{R}^4$$

It follows from (31) and (38) that:

$$\psi_0(W_0) = \begin{pmatrix} -k_1 w_{1,0} \\ -\psi_{1,0}(W_0) \\ w_{2,0} \\ k_2(k_p w_{2,0} + k_i w_{3,0} - w_{4,0}) \end{pmatrix} \tag{39}$$

where

$$\begin{aligned} \psi_{1,0}(W_0) &= \lim_{\varepsilon\to 0} \frac{1}{2\pi} \int_0^{2\pi} \psi_1(W(\tau)) d\tau \\ &= \frac{w_{4,0} E_g^2}{C}[(1 - r_g w_{4,0} - (L_g + L)k_2(k_p w_{2,0} + \\ &k_i w_{3,0} - w_{4,0})] + \frac{w_{4,0} E_g I_{L1} \omega_g}{C}(L_g + L) sin(\varphi_1) \\ &- \frac{E_g I_{L1}}{C}[1 - r_g w_{4,0} - (L_g + L)k_2(k_p w_{2,0} + \\ &k_i w_{3,0} - w_{4,0})] \cos(\varphi_1) \end{aligned} \tag{40a}$$

$$\psi_{2,0}(W_0) = \lim_{\varepsilon\to 0} \frac{1}{2\pi} \int_0^{2\pi} \psi_2(\tau, W, \varepsilon) d\tau = 0 \tag{40b}$$

where $w_{i,0} (i = 1, \dots 4)$ are the elements of the vector W_0.

The stability analysis of (37) will be performed by analyzing its equivalent averaged system that given by:

$$\dot{W}_0 = \varepsilon\psi_0(W_0) \tag{41}$$

It is worth to note that for a given $\psi_{1,0}(W_0)$ in (39), only one equilibrium W_0^* exists for the nonlinear system (41) which is given by the following expression:

$$W_0^* = \begin{pmatrix} 0 & 0 & \frac{\beta_0}{k_i} & \beta_0 \end{pmatrix}^T \tag{42}$$

with

$$\beta_0 = \frac{b_2 + \sqrt{b_2^2 - 4b_1 b_3}}{2b_1} \tag{43}$$

The stability analysis of the equilibrium point ${W_0}^*$ can be performed by using the indirect Lyapunov method [33]. Therefore, one can verify wether the Jacobian M of the function $\psi_0(.)$ at W_0^* is Hurwitz. According to (39)-(41), the Jacobian matrix M can be expressed as follows:

$$M = \begin{pmatrix} -k_1 & 0 & 0 & 0 \\ 0 & k_2 k_p b_4 & k_2 k_i b_4 & -b_5 \\ 0 & 1 & 0 & 0 \\ 0 & k_2 k_p & k_2 k_i & -k_2 \end{pmatrix} \tag{44}$$

The equilibrium ${W_0}^*$ would be globally asymptotically stable if the matrix M is Hurwitz, i.e if the roots of its characteristic polynomial are in the left hand side of the complex plane. The characteristic polynomial of the Jacobian matrix can be expressed as follows:

$$\Pi(\lambda) = \lambda^4 + a_3\lambda^3 + a_2\lambda^2 + a_1\lambda + a_0 \tag{45}$$

where coefficients a_0, a_1, a_2, and a_3 are given in Table I.

By using the Routh-Hurwitz criterion, it turns out that all the roots of the characteristic polynomial (45) lie in the left hand side of the complex plane when the conditions (36) are satisfied. i.e. the equilibrium ${W_0}^* = W_0$ of (41) is exponentially stable. Applying (Theorem 10.4 in [33]), we obtain that the system (37) has a solution $\bar{Z}(t, \varepsilon)$ fulfilling the inequality (36).

VI. Numerical simulation

To validate the previous theoretical results, in this section, the performance of the designed nonlinear controller will be tested by performing numerical simulation using the switched model of the HBIB-SAPF depicted in figure 3. The simulation was performed by using Matlab/SimPower Systems environment by selecting the solver ODE14x (Extrapolation) with a fixed step time of $1\,\mu$s. The parameter values of the HBIB-SAPF are summarized in Table II.

- **Simulation considerations**

The previous choice of the DC capacitor voltage at the output converter is motivated by the purpose of reducing well the oscillations of DC bus voltage v_{dc}, which are imposed by the lower order harmonics or unbalanced of linear/ nonlinear loads. To this end, the capacitance value at the DC side must

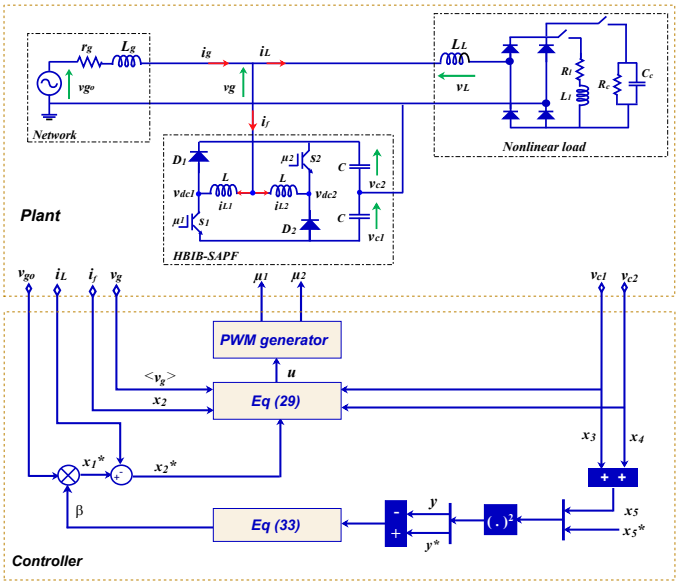

Fig. 3. Global simulated system with cascade nonlinear controller.

be sufficiently large. The DC bus capacitor and the inductor designs are selected following the method proposed in [34].

On the other hand, the implementation of the nonlinear controller, including the internal loop control law (29) and the external loop control laws (33) and (34), depends mainly on the controller parameters k_1, k_2, k_p and k_i. Bearing in mind that the numerical values of these parameters must be selected in such a way that the inequalities in (36) are met. The main challenge comes from the fact that there is no systematic way, especially in nonlinear control to suitably select these values. Therefore, the usual practice consists in proceeding with a trial-error approach. Nevertheless, it can be easily seen that, if both parameters (k_1, k_2) are fixed, then (36) sums up to a set of linear inequalities in terms of parameters k_p and k_i. These inequalities are readily re-written to a simple linear matrix inequality (LMI), which is treated using the Matlab LMI toolbox. According to the above procedure, the numerical values of Table III are obtained. The values of the characteristic polynomial coefficients $a_i; i = 0, ...3$ are listed in Table IV. They meet conditions (36).

For checking the performances of the system, the following cases are considered:

- Control performance in presence of nonlinear load,
- Control performance in presence of varying DC voltage reference,
- Control performance in presence of supply grid voltage changes,
- Control performance with system parameters variation,
- Comparison with a hybrid controller under load changes.

A. Control performance in presence of nonlinear load

The performances of the proposed controller are checked under a nonlinear load. This latter is composed of a full-bridge rectifier feeding a load constituted by a resistor R_{l1} in series with an inductor L_1. Figures 4a and 4b show the load current i_L (time domain waveform and its FFT spectrum, respectively). It is seen that this load current is highly rich in harmonic components, where its THD value is found to be 44.72%. The simulation results are illustrated by Figure 5 which demonstrates the most significant aspect of the system behavior. In fact, figure 5a shows that the injected filter current into the grid tracks its reference signal with good accuracy, resulting in strong steady-state behavior and a rapid dynamic response of the backstepping controller. Figure 5b shows that the grid current becomes in sinusoidal waveform and in phase

TABLE II
POWER SYSTEM PARAMETERS.

Parameters	*Symbol*	*Values*
Grid	E_g	$110\sqrt{2}$ V
	f_g	50 Hz
	r_g,L_g	70 mΩ, 1 mH
Nonlinear load	R_l, L_l	10 Ω, 150 mH
	R_c, C_c	20 Ω, 2 mH
HBIB-SAPF	C	2.2 mF
	L	2 mH
	L_L	0.5 mH

TABLE III
CONTROLLER PARAMETERS.

Parameters	*Symbol*	*Values*
PWM switching frequency	f	10 kHz
Current regulator	k_1	$1000\,s^{-1}$
Voltage regulator	k_p	3.2×10^{-6}
	k_i	1.64×10^{-4}
	k_2	$2 \times 10^{3}\,s^{-1}$

TABLE IV
THE VALUES OF COEFFICIENTS a_i WITH $i = 0, ...3$.

a_0	a_1	a_2	a_3
1.5011×10^{11}	2.9254×10^{9}	1.7765×10^{6}	1.1520

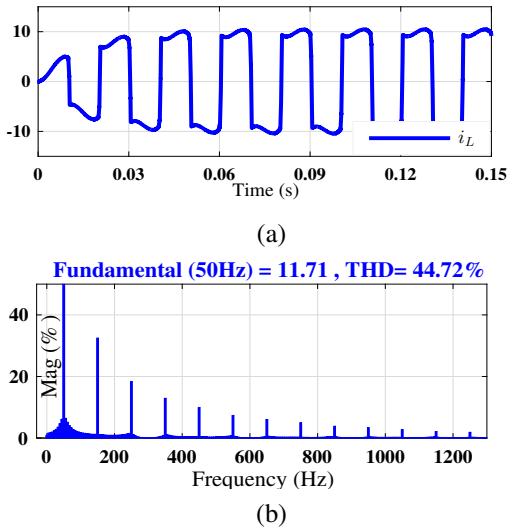

Fig. 4. (a) Load current i_L in time domain, (b) FFT spectrum.

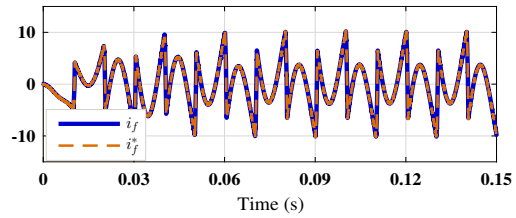

(a) i_f and its reference i_f^*.

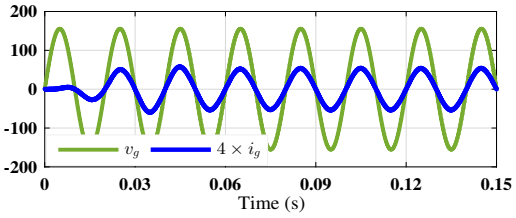

(b) Grid voltage v_g and current i_g showing good PFC.

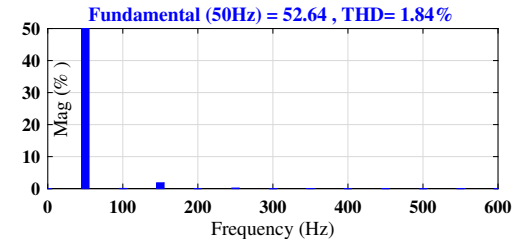

(c) FFT spectrum of the grid current.

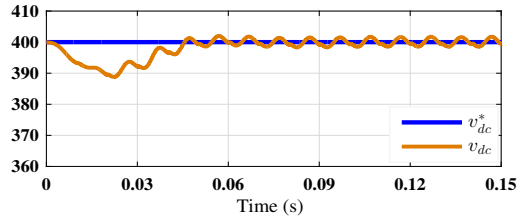

(d) Output voltage v_{dc}.

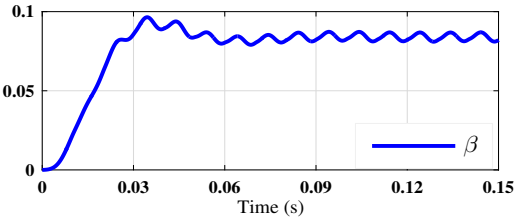

(e) Control signal β

Fig. 5. Simulation results under nonlinear load.

with the grid voltage, which confirms the achievement of the unity power factor objective. The FFT spectrum of the grid current shows also that the harmonics have well compensated for, where its THD value is equal to 1.84% (see figure 5c). Figure 5d shows that the DC voltage reaches its reference value ($v_{dc}^* = 400\,\mathrm{V}$) after a short transient time. One can also observe that the DC voltage holds ripples, but they are less than 1% of v_{dc}. These oscillations are a natural behavior due to DC-AC energy conversion. Hence, they are inevitable whenever the power factor correction is provided regardless of the control design. Figure 5e shows the control signal β. Note that after a short transient, this signal takes a practically constant value guaranteeing a near unitary power factor.

B. Control performance in presence of varying DC voltage reference

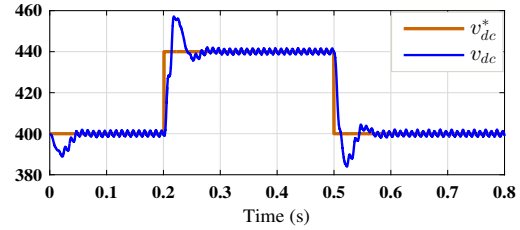

(a) Output voltage v_{dc}.

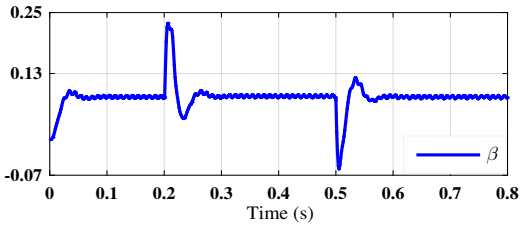

(b) Control signal β.

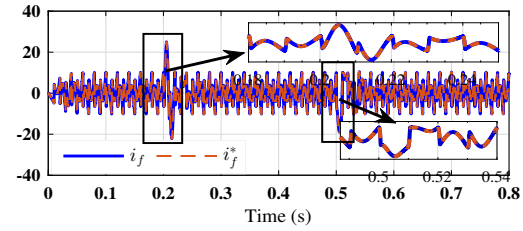

(c) Filter current i_f and its reference i_f^*.

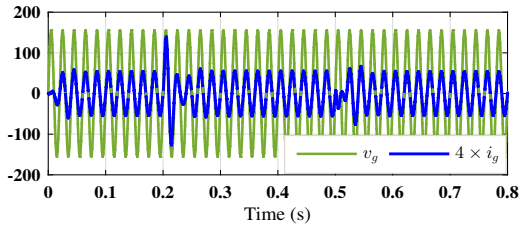

(d) Grid voltage v_g and current i_g showing PFC.

Fig. 6. Simulation results under voltage step changes.

The controller performances are tested considering the voltage reference change. More specifically, the voltage reference v_{dc}^* steps from $400\,\mathrm{V}$ to $440\,\mathrm{V}$ at $0.2\,\mathrm{s}$ and then back to $400\,\mathrm{V}$. Figure 6 illustrates the resulting controller behavior. As explained in Theorem 1, the output DC voltage v_{dc} converges, in the average, to its reference value with a good accuracy (see figure 6a). Besides, it is observed that the voltage ripples oscillate at the frequency $2\omega_g$, but their amplitudes are negligible compared to the average value of the signals,

proving thus Theorem 1. Figure 6b depicts that the signal of the external loop β stabilizes after a short transient period according to the change of the voltage reference. Figure 6c illustrates the current waveform that delivered by the HBIB-SAPF. In figure 6d, it is clear that the waveform of the grid current is maintained sinusoidal and in phase with the grid voltage, except for a brief period of time (0.03 s) after the v_{dc}^* change.

C. Control performance in presence of supply grid voltage changes

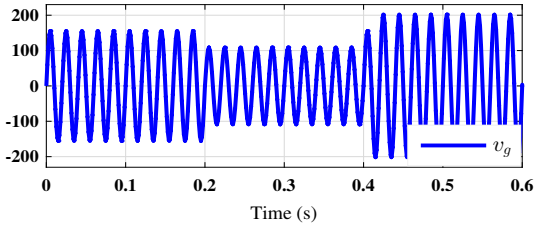

(a) v_g waveform under $\pm 30\%$ change of its nominal value.

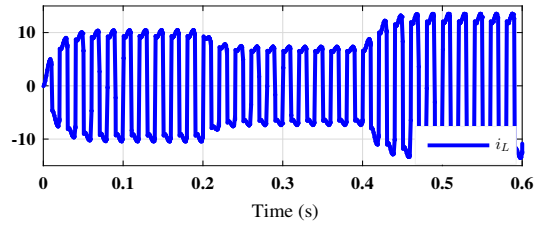

(b) Load current i_L waveform.

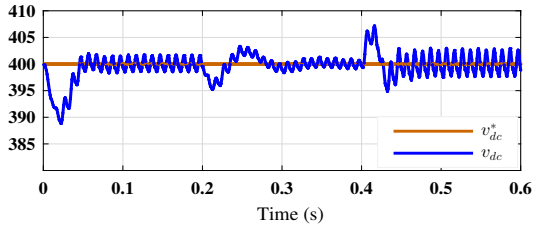

(c) Output voltage v_{dc}.

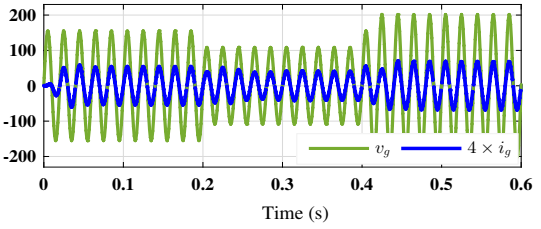

(d) Grid voltage v_g and current i_g showing a perfect PFC.

Fig. 7. Simulation results under supply grid voltage changes.

In this case study, the simulation aims at illustrating the behavior of the double-loop control system in the presence of voltage level variations in the electric power grid. To this end, the magnitude of input grid voltage undergoes a deviation of $\pm 30\%$ from its nominal value $E_g = 110\sqrt{2}$ V as shown in figure 7a. Specifically, the grid voltage level is changed in accordance with the following process:

- 30% decrease at time 0.2 s.
- 30% increase at time 0.4 s.

It is worth noting that the change in the grid voltage level is only used in the simulation model. The regulator is not suited to account for these variations, that is, a fixed regulator is used permanently, derived from the system nominal values. The simulation results are illustrated by figure 7. The findings demonstrate that the proposed regulator is robust against the grid voltage perturbation. In particular, the voltage regulator guarantees that the DC voltage is recovered to the reference level with a short response time depending on the change and the average steady-state tracking error is null as illustrated in figure 7c. The current controller ensures that the PFC is well performed with low THD values. This is proven in figure 7d where the grid voltage and current are still sinusoidal and in the same phase all the time despite of power grid level changes.

TABLE V
THD OF MITIGATED GRID CURRENT.

Nonlinear RL load		
with E_g	-30% E_g	+30%E_g
Before connecting HBIB-SAPF		
44.72%	42.80%	43.85%
After connecting HBIB-SAPF		
0.93%	1.84%	3.39%

The THD values of mitigated grid current resulted from the HBIB-SAPF system are summarized in figure V. The findings confirm that the proposed controller performs successfully under different operating conditions, resulting in low THD values below 5% that complies with the limit set by IEEE Standard [6].

D. Control performance with system parameters variation

The effectiveness of the designed cascade controller is tested under the parameter uncertainties of the LC filter. The simulation profile is illustrated by Figures 8a and 9a, which show that the capacitance C and inductance L are subject to decrease at 0.2 s and to increase at 0.4 s. Other than this variation, the remainder of the system features are the same as in Tables II and III. The obtained results (figures8 and 9) show that despite the LC-filter component uncertainties, the deterioration of control performances remains quite limited. In the case of the capacitance C variation, figure 8b depicts that the DC voltage holds constant in average, equal to the reference value 400 V. It can also be seen that, over the capacitance change interval, the voltage ripples decrease as the value of C is increased and vice versa. Figure 8c indicates that the external loop control β is constant, but is also influenced by the variation of the C parameter values similarly to the DC bus voltage. Figures 8d and 8e show that the harmonics and reactive compensation are well performed, while the inner loop control signal u is not influenced by the uncertainty on the capacitance C.

In the case of inductance L variation, it can be seen from figures (9a-9e) that there is no deterioration of the controller

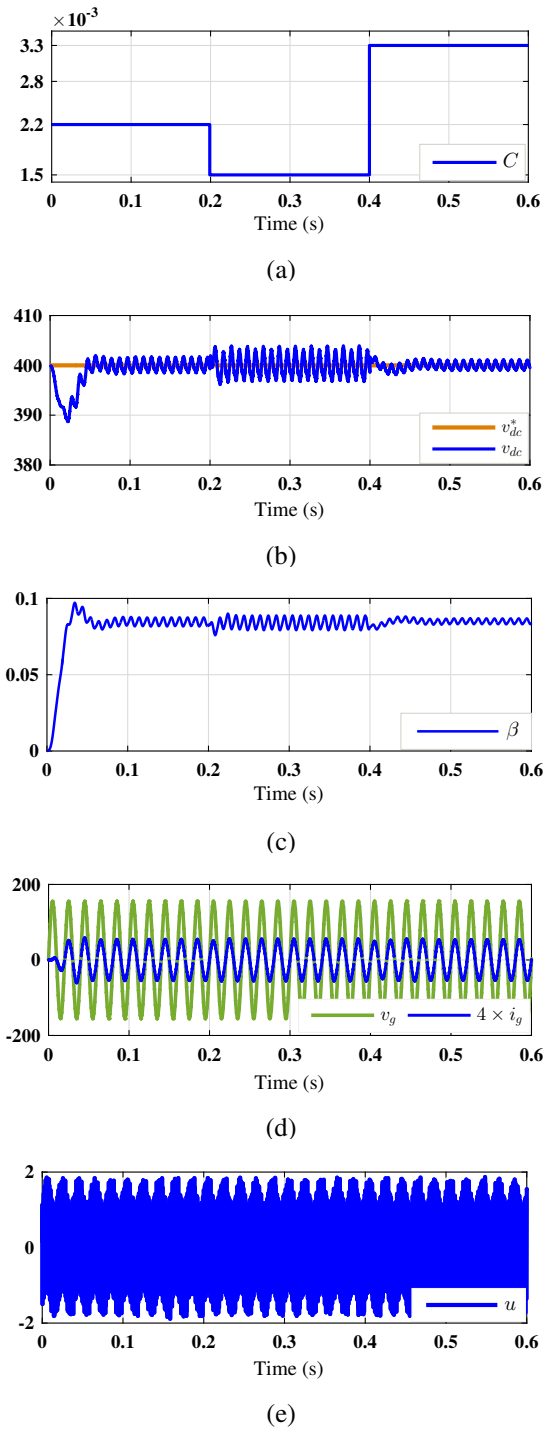

Fig. 8. Illustration of controller robustness against capacitance uncertainty: (a) capacitor change, (b) output voltage v_{dc}, (c) control signal β, (d) power factor checking and (e) control signal u.

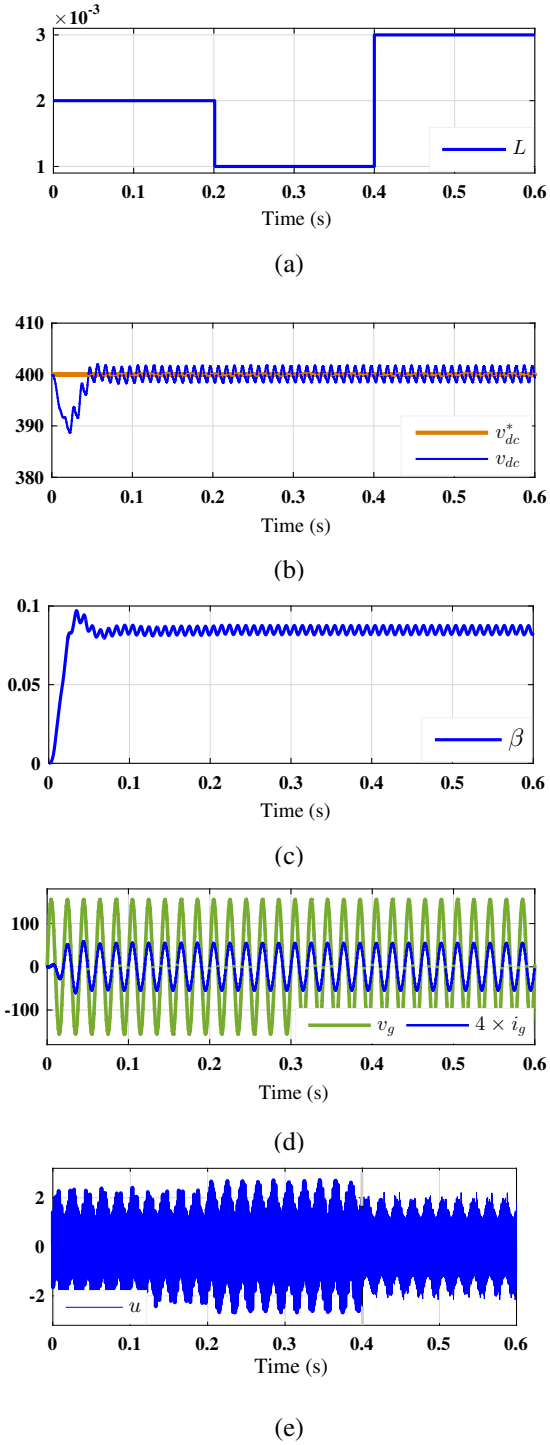

Fig. 9. Illustration of controller robustness against inductance uncertainty: (a) inductor change, (b) output voltage v_{dc}, (c) control signal β, (d) power factor checking, and (e) control signal u.

performances. Specifically, the DC voltage and signal β keep unaltered on the uncertainty interval (figures 9b and 9c). However, a rather small undulations occurs on the grid current (figure 9d) as well as on the inner loop control signal u (figure 9e) during the interval of uncertainty.

E. Comparison with a hybrid controller under load changes

The performance and robustness of the proposed nonlinear controller are tested and evaluated under load changes and compared with those corresponding to a hybrid automaton controller [17]. This comparative study is performed using two nonlinear loads. The first one is constructed using an AC/DC converter feeding a parallel resistor R_c and capacitor

C_c (capacitive). The second nonlinear load is developed using the same converter feeding a series connected resistor R_l and an inductor L_l (inductive load).

In this simulation test, the load varies from the first nonlinear load to the second nonlinear at time $0.3\,\mathrm{s}$. The resulting performances of both controllers are illustrated by figures (10-14). The load current waveform i_L in presence of load changes is illustrated in figure 10. Figures 11 and 12 show the responses of each controller in current harmonics mitigation. It is clearly observed that the proposed nonlinear controller shows better dynamic performances with a settling time of $0.07\,\mathrm{s}$, proving that the filter current tracks well its reference signal (Fig. 11a). Therefore, the compensation of harmonic currents and reactive power is perfectly performed as proved by the obtained sinusoidal grid current, with a reduced THD, and in phase with the grid voltage. Meanwhile, the hybrid automaton controller performs with a larger settling time of $0.11\,\mathrm{s}$.

On the other hand, figures 13 and 14 show the responses corresponding to each controller in terms of DC voltage regulation. In fact, the filtered-PI proposed in this work shows satisfactory results as can be observed in figure 13a, where the DC capacitor voltage is recovered and achieves its reference v_{dc}^* after a short transient time of $0.1\,\mathrm{s}$, with overshoot of $15\,\mathrm{V}$. In turn, the outer loop control signal β rapidly reaches its steady-state after load change (see figure. 13b), guaranteeing unitary power factor. However, the simple PI regulator that is used in other method performs poorly with high overshoot of $18.5\,\mathrm{V}$ and a larger settling time of $0.15\,\mathrm{s}$ following the load changes.

THD values of grid current i_g resulted from SAPF utilizing each controller are depicted in Table VI. The results clearly show that each controller has successfully removed the current harmonics generated by all nonlinear loads, resulting in THD values of far below 5%, conforming with the limit set by Standard IEEE 519-2014. However, the proposed nonlinear backstepping controller with filtered PI performs outstandingly by achieving the lowest THD values for two nonlinear loads.

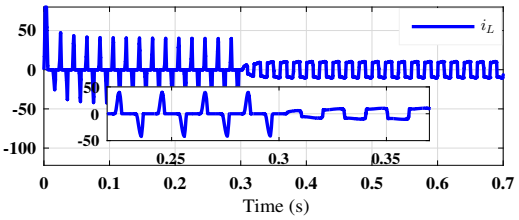

Fig. 10. Load current i_L under load change.

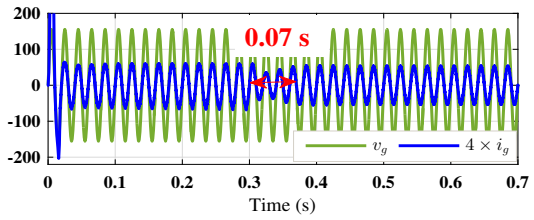

(a) PFC checking

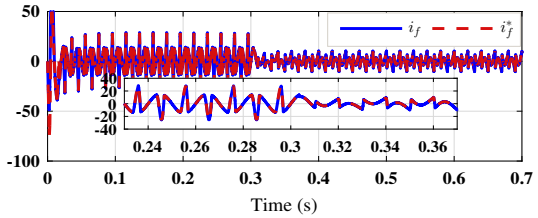

(b) current filter i_f and its reference i_f^*.

Fig. 11. Dynamic response of backstepping controller.

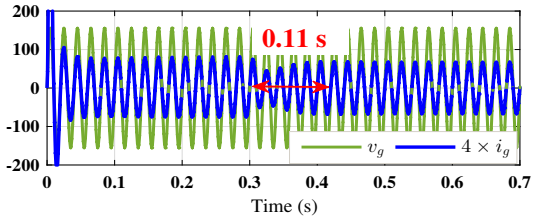

(a) Grid current and voltage showing PFC.

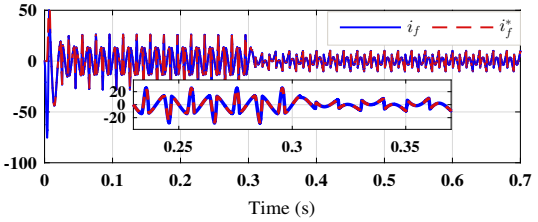

(b) current filter i_f and its reference i_f^* .

Fig. 12. Dynamic response of hybrid controller.

TABLE VI
THDS OF MITIGATED GRID CURRENT FOR EACH CONTROLLER.

Control strategies	**Total Harmonic Distortion, (THD %)**	
	Bridge R_lL_l	***Bridge*** R_cC_c
	Before connecting HBIB-SAPF	
	44.72%	108.14%
	After connecting HBIB-SAPF	
Nonlinear control	0.93%	2%
Hybrid control	1.5%	2.6%

VII. CONCLUSION

This work dealt with the problem of controlling a single-phase shunt active power filter based on half-bridge interleaved buck converter. As a first step, an equivalent average model was proposed in which the filter system dynamics was described by the 4^{th} order nonlinear state-space representation. Then, on the basis of such a model, a nonlinear cascade controller was designed using various tools from control theory like, system averaging theory and Lyapunov design. The results obtained in numerical simulation as well as in theoretical analysis demonstrate that the developed nonlinear controller performs well in terms of tracking and robustness against uncertainty. Finally, it was formally proven that the overall system is globally asymptotically stable and that the control requirements are met, including i) compensation of

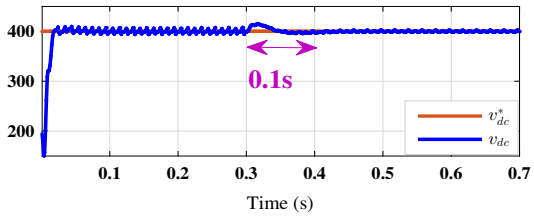

(a) DC voltage v_{dc} and its reference v_{dc}^*

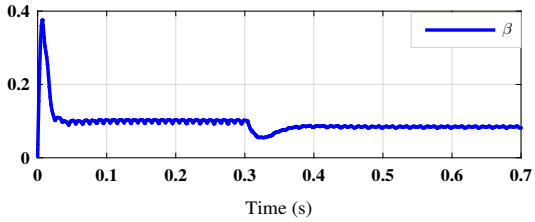

(b) Control signal β.

Fig. 13. Dynamic behavior of filtered PI regulator.

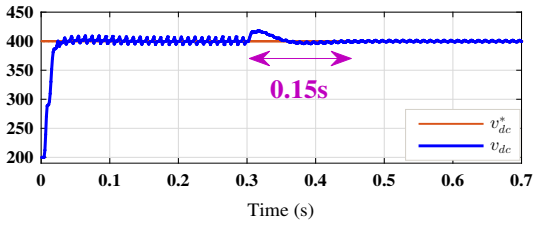

(a) DC voltage v_{dc} and its reference v_{dc}^*

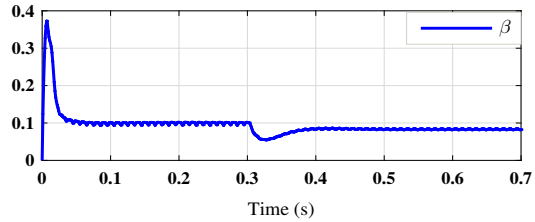

(b) Control signal β.

Fig. 14. Dynamic behavior of simple PI regulator.

harmonics and reactive power absorbed by the nonlinear loads; ii) a tight voltage regulation at the half-bridge interleaved buck converter output capacitor.

Appendix. Proof of the equation (32)

The relationship between β and x_5 is given by the following expressions:

$$f_1(\beta,\dot{\beta}) = \frac{\beta E_g^2}{C}\left(1 - r_g\beta - (L_g+L)\dot{\beta}\right) - \frac{E_g I_{L1}}{C}\Big[1 - r_g\beta - (L_g+L)\dot{\beta}\Big]\cos(\varphi_1) + \frac{\beta E_g I_{L1}\omega_g}{C}(L_g+L)\sin(\varphi_1) \tag{46}$$

$$f_2(\beta,\dot{\beta},Z,t) = -\frac{\beta E_g^2}{C}\left(1 - r_g\beta - (L_g+L)\dot{\beta}\right)\cos(2\omega_g t) - \frac{E_g^2\beta^2\omega_g}{C}(L_g+L)\sin(2\omega_g t) + \frac{2E_g}{C}\Bigg[\beta\left(L_L\frac{di_L}{dt} + k_1 z_1\right) + \left(\beta\omega_g(L_g+L) - \left(1 - r_g\beta - (L_g+L)\dot{\beta}\right)\right)\sum_{h=2}^{\infty} I_{Lh}\sin(h\omega_g t + \varphi_h)\Bigg]\sin(\omega_g t) + \frac{E_g I_L}{C}\left(1 - r_g\beta - (L_g+L)\dot{\beta}\right)\cos(2\omega_g t + \varphi_1) + \frac{\beta E_g I_L\omega_g}{C}(L_g+L)\sin(2\omega_g t + \varphi_1) - \frac{2L_L}{C}\frac{di_L}{dt}iL(t) - \frac{2}{C}(k_1 z_1)i_L(t) \tag{47}$$

Acknowledgement

M. Al-Numay and A. El Aroudi acknowledge financial support from the Researchers Supporting Project number (RSP-2021/150), King Saud University, Riyadh, Saudi Arabia.

References

[1] A. Kalair, N. Abas, A. R. Kalair, Z. Saleem, and N. Khan, "Review of harmonic analysis, modeling and mitigation techniques," *Renewable and Sustainable Energy Reviews*, vol. 78, pp. 1152–1187, oct 2017.

[2] Z. Hekss, A. Abouloifa, I. Lachkar, F. Giri, S. Echalih, and J. M. Guerrero, "Nonlinear adaptive control design with average performance analysis for photovoltaic system based on half bridge shunt active power filter," *International Journal of Electrical Power and Energy Systems*, vol. 125, feb 2021.

[3] A. Abouloifa, F. Giri, I. Lachkar, F. Z. Chaoui, M. Kissaoui, and Y. Abouelmahjoub, "Cascade nonlinear control of shunt active power filters with average performance analysis," *Control Engineering Practice*, vol. 26, no. 1, pp. 211–221, 2014.

[4] Z. Hekss, A. Abouloifa, S. Echalih, and I. Lachkar, "Cascade nonlinear control of photovoltaic system connected to single phase half bridge shunt active power filter," in *Proceedings of 2019 IEEE World Conference on Complex Systems, WCCS 2019*. 2019 4th World Conference on Complex Systems (WCCS), 2019.

[5] O. P. Mahela and A. G. Shaik, "Topological aspects of power quality improvement techniques: A comprehensive overview," *Renewable and Sustainable Energy Reviews*, vol. 58, pp. 1129–1142, 2016.

[6] "Ieee recommended practice and requirements for harmonic control in electric power systems," *IEEE Std 519-2014 (Revision of IEEE Std 519-1992)*, pp. 1–29, 2014.

[7] S. Kumaresan and H. Habeebullah Sait, "Design and control of shunt active power filter for power quality improvement of utility powered brushless DC motor drives," *Automatika*, vol. 61, no. 3, pp. 507–521, jul 2020.

[8] Y. Terriche, J. M. Guerrero, and J. C. Vasquez, "Performance improvement of shunt active power filter based on non-linear least-square approach," *Electric Power Systems Research*, vol. 160, pp. 44–55, Jul. 2018.

[9] S. Abe, K. Hasegawa, M. Tsukuda, K. Wada, I. Omura, and T. Ninomiya, "Modelling of the shoot-through phenomenon introduced by the next generation igbt in inverter applications," *Microelectronics Reliability*, vol. 76, pp. 465–469, 2017.

[10] U. Abronzini, C. Attaianese, M. D'Arpino, M. D. Monaco, and G. Tomasso, "Steady-state dead-time compensation in vsi," *IEEE Transactions on Industrial Electronics*, vol. 63, no. 9, pp. 5858–5866, 2016.

[11] Z. Zhang and L. Xu, "Dead-time compensation of inverters considering snubber and parasitic capacitance," *IEEE Transactions on Power Electronics*, vol. 29, no. 6, pp. 3179–3187, 2014.

[12] P. Sun, C. Liu, J.-S. Lai, and C.-L. Chen, "Cascade dual buck inverter with phase-shift control," *IEEE Transactions on Power Electronics*, vol. 27, no. 4, pp. 2067–2077, Apr. 2012.

[13] P. Sun, C. Liu, J.-S. Lai, C.-L. Chen, and N. Kees, "Three-phase dual-buck inverter with unified pulsewidth modulation," *IEEE Transactions on Power Electronics*, vol. 27, no. 3, pp. 1159–1167, Mar. 2012.

[14] F. Hong, J. Liu, B. Ji, Y. Zhou, J. Wang, and C. Wang, "Interleaved dual buck full-bridge three-level inverter," *IEEE Transactions on Power Electronics*, vol. 31, no. 2, pp. 964–974, Mar. 2016.

[15] Y. Cho, "Dual-buck residential photovoltaic inverter with a high-accuracy repetitive current controller," *Renewable Energy*, vol. 101, pp. 168–181, 2017.

[16] Z. Fu, Z. Feng, X. Chen, and X. Zheng, "High-reliability three-phase dual-buck grid-connected inverter without shoot-through problem," *Journal of Power Electronics*, vol. 19, no. 2, pp. 454–462, 2019.

[17] S. Echalih, A. Abouloifa, I. Lachkar, Z. Hekss, M. Aourir, and F. Giri, "Hybrid control of single phase shunt active power filter based on interleaved buck converter." 2019 American Control Conference (ACC), IEEE, July 2019, pp. 3636–3641.

[18] S. Echalih, A. Abouloifa, Z. Hekss, and I. Lachkar, "Half wave control strategy of interleaved buck converter based single phase active power filter for power quality improvement." 2019 4th World Conference on Complex Systems (WCCS), April 2019, pp. 1–6.

[19] R. Patel, A. K. Panda, and A. Kumar, "Real-time analysis of fuzzy controlled 2C dual buck half-bridge shunt APF with different MFs for dynamic unbalanced load," 2018 Technologies for Smart-City Energy Security and Power (ICSESP). Bhubaneswar: IEEE, Mar. 2018, pp. 1–6.

[20] R. Patel and A. K. Panda, "Real Time harmonic mitigation using fuzzy based highly reliable three dual-buck full-bridge APF for dynamic unbalanced load," *International Journal of Emerging Electric Power Systems*, vol. 19, no. 3, Jun. 2018.

[21] A. K. Panda and R. Patel, "PI and fuzzy-controlled 3-phase 4-wire interleaved buck active power filter with shoot-through elimination for power quality improvement using RTDS hardware," *International Journal of Emerging Electric Power Systems*, vol. 15, no. 2, pp. 177–194, Apr. 2014.

[22] R. Patel and A. K. Panda, "Adaptive hysteresis and fuzzy logic controlled based shunt active power filter resistant to shoot-through phenomenon," *IET Power Electronics*, vol. 8, no. 10, pp. 1963–1977, Oct. 2015.

[23] A. K. Panda and S. Mikkili, "FLC based shunt active filter (p–q and id–iq) control strategies for mitigation of harmonics with different fuzzy MFs using matlab and real-time digital simulator," *Electrical Power and Energy Systems*, vol. 47, p. 313–336, 2013.

[24] V. Gali, N. Gupta, and R. A. Gupta, "PTF-based control algorithm for three-phase interleaved inverter-based sapf," *International Journal of Electronics*, vol. 106, no. 7, pp. 1060–1084, 2019.

[25] S. Echalih, A. Abouloifa, J. Janik, I. Lachkar, Z. Hekss, F. Chaoui, and F. Giri, "Hybrid Controller with Fuzzy Logic Technique for Three Phase Half Bridge Interleaved Buck Shunt Active Power Filter," *IFAC-PapersOnLine*, vol. 53, no. 2, 2020.

[26] S. Echalih, A. Abouloifa, I. Lachkar, J. M. Guerrero, Z. Hekss, and F. Giri, "Hybrid automaton-fuzzy control of single phase dual buck half bridge shunt active power filter for shoot through elimination and power quality improvement," *International Journal of Electrical Power and Energy Systems*, vol. 131, p. 106986, 2021.

[27] V. Gali, N. Gupta, and R. A. Gupta, "Enhanced particle swarm optimization based dc-link voltage control algorithm for interleaved sapf," *Journal of Engineering Science and Technology*, vol. 13, no. 10, pp. 3393–3418, 2018.

[28] V. Gali, N. Gupta, and R. Gupta, "Enhanced particle swarm optimization technique for interleaved inverter tied shunt active power filter," in *Soft Computing for Problem Solving*. Springer, 2019, pp. 571–583.

[29] V. Gali, N. Gupta, and R. A. Gupta, "Experimental investigations on multitudinal sliding mode controller-based interleaved shunt apf to mitigate shoot-through and pq problems under distorted supply voltage conditions," *International Transactions on Electrical Energy Systems*, vol. 29, no. 1, p. e2701, 2019.

[30] Z. Hekss, A. Abouloifa, J. Janik, I. Lachkar, S. Echalih, F. Chaoui, and F. Giri, "Hybrid Automaton Control of Three Phase Reduced Switch Shunt Active Power Filter Connected Photovoltaic System," *IFAC-PapersOnLine*, vol. 53, no. 2, 2020.

[31] Z. Hekss, I. Lachkar, A. Abouloifa, S. Echalih, M. Aourir, and F. Giri, "Nonlinear control strategy of single phase half bridge shunt active power filter interfacing renewable energy source and grid," in *Proceedings of the American Control Conference*, vol. 2019-July. 2019 American Control Conference (ACC), IEEE, 2019.

[32] Z. Chen and M. Chen, "Optimal control strategy of the interleaved buck cell based shunt active filter." IECON 2012-38th Annual Conference on IEEE Industrial Electronics Society, 2012, pp. 4457–4462.

[33] H. K. Khalil, *Nonlinear systems, 3rd ed.* Prentice hall Upper Saddle River, NJ, 2002.

[34] J. Chen and X. Zhang, "Study on the power quality of more electric aircraft power grid." 2016 18th European Conference on Power Electronics and Applications, EPE 2016 ECCE Europe, 2016.

Salwa Echalih received her master's degree in data processing from the Faculty of Sciences Ben M'sick, Hassan II University of Casablanca, Morocco, in 2017. Currently, she is preparing her Ph.D. in the field of automatic control, renewable energies and power electronics at Hassan II University of Casablanca, Morocco. Her research interests include power quality improvement of electrical energy, renewable energy systems, nonlinear control techniques, and hybrid control of active power filter based on interleaved buck converter.

Abdelmajid Abouloifa received his Ph.D. in control engineering from the University of Caen Basse-Normandie, Caen, France in 2008. He is currently Professor at National School of Electricity and Mechanic, Hassan II University of Casablanca. His main research areas include modeling, nonlinear control, observation of FACTS systems, actives filters, uninterruptible power supplies, and photovoltaic systems.

Ibtissam Lachkar received the graduate degree from the Normal High School of Technical Education, Rabat, Morocco, in 1995 and her degree of high depth studies from the Mohammedia School of Engineers, Rabat, in 2005. She received her Ph.D. from Mohammedia School of Engineers. Currently, she is a Professor at National School of Electricity and Mechanic. Her research interests include modeling, nonlinear control, uninterruptible power supplies, and photovoltaic systems.

Zineb Hekss received her master's degree in data processing from the Faculty of Sciences Ben M'sick, Hassan II University of Casablanca, Morocco, in 2017. Currently, she is preparing her Ph.D. in the field of automatic control, renewable energies and power electronics at Hassan II University of Casablanca, Morocco. Her research interests include renewable energy systems, power quality improvement of electrical energy, modeling, observation and nonlinear control techniques of active power filter associated with a photovoltaic system.

Fouad Giri received his Ph.D. in Automatic Control from Institut National Polytechnique de Grenoble, Grenoble, France, in 1988. He is currently Professor at the University of Caen Normandie, France. His research interests include nonlinear system identification, observation and control, and application to power electric systems.

Abdelali El Aroudi received his Ph.D degree in applied physical science from the Universitat Politècnica de Catalunya, Barcelona, Spain, in 2000. He is currently Professor at the Universitat Rovira i Virgili (URV), Tarragona, Spain. His research interests include the field of structure and control of power conditioning systems for autonomous systems, power factor correction, renewable energy applications, stability problems, nonlinear phenomena, and bifurcations control.

Mohammmed Al-Numay He received the B.S. degree (with honors) from King Saud University, Riyadh,Saudi Arabia, in 1986, the M.S. degree from Michigan State University, East Lansing, MI, in 1990,and the Ph.D. degree from Georgia Institute of Technology, Atlanta, GA, in 1997, all in electrical engineering. Since 1998, he has been with the Electrical Engineering Department at King Saud University, where he is now a Professor. During the period 2002-2006, he was the Dean of Admissions and Registration at King Saud University. From 2008 until now, he is a Senior Consultant of Student Information Systems (SIS) and electronic admission to many governmental and private universities and colleges. He was appointed asthe Vice Rector for Educational and Academic Affairs for the same university in 2017. His research interests include modeling, analysis, design and control of power electronics